# Optical techniques for real-time penetration monitoring for laser welding

Fabrice Bardin, Adolfo Cobo, Jose M. Lopez-Higuera, Olivier Collin, Pascal Aubry, Thierry Dubois, Mats Högström, Per Nylen, Peter Jonsson, Julian D. C. Jones, and Duncan P. Hand

Optical techniques for real-time full-penetration monitoring for Nd:YAG laser welding have been investigated. Coaxial light emission from the keyhole is imaged onto three photodiodes and a camera. We describe the spectral and statistical analyses from photodiode signals, which indicate the presence of a full penetration. Two image processing techniques based on the keyhole shape recognition and the keyhole image intensity profile along the welding path are presented. An intensity ratio parameter is used to determine the extent of opening at the rear of a fully opened keyhole. We show that this parameter clearly interprets a hole in formation or a lack of penetration when welding is performed on workpieces with variable thicknesses at constant laser power. 

*OCIS codes:* 140.3390, 040.0040, 060.2370, 100.2960.

## 1. Introduction

Laser welding is of increasing interest for aeronautics applications, particularly because of the inherent low distortion of the process and its suitability for automation. However, in such safety-critical applications, it is vital that every weld can be assured to be free of defects; hence the requirement for process monitoring and control in order to detect (and where feasible, eliminate) possible defects in the weld (e.g., lack of penetration or porosities). Such a system would ensure a consistent process and reduce scrap and rework. It may ultimately also be possible to reduce the (currently stringent) requirements for nondestructive testing.

Several sensors have been investigated, based on visible, infrared, ultraviolet, x-ray and acoustic analysis. A small number of optical-based online monitoring systems, based on cameras or photodiodes, have been commercialized for several years (for instance, Plasmo from ARC Seibersdorf research GmbH, Laser Welding Monitor LWM from Precitec, Welding monitor PD 2000 from Prometec,[1] Weldwatcher from 4D,[2] Porosearch/LW, and tracking systems from ServoRobot). The majority of actual systems use single-point photodiodes, because they are relatively inexpensive and produce a small amount of data while having a high temporal resolution. Most of the strategies developed detect the fluctuations of plasma emissions and compare them with a reference, which leads to difficulties in distinguishing between a large number of different possible defects (pore, lack of penetration, hole, gap, and oxidation). Real-time full-penetration monitoring can be achieved by observation of the root-side light emission,[3,4] by detection of the frequency oscillations of an opened keyhole,[5,6] or by using sensor fusion associated with statistical and spectral measurements.[4,7] The degree of partial penetration can be estimated by coaxially monitoring the optical signals emitted from the weld-pool area, since there exists a linear correlation between penetration depth and the optical signals.[8,9] The main drawback of using single-point photodiodes is the complete loss of the weld-pool spatial information, whereas CCD cameras offer a high spatial resolution. However, affordable CCD cameras have a very low temporal resolution and thus cannot follow rapid fluctuations. Recently emerging CMOS cameras allow smaller im-

F. Bardin (f.bardin@hw.ac.uk), J. D. C. Jones and D. P. Hand are with the School of Engineering and Physical Sciences, Heriot-Watt University, Edinburgh, EH14 4AS, U.K. A. Cobo and J. M. Lopez-Higuera are with the Universidad Cantabria, Avenida de los Castros, s/n, Santander, E-39005, Spain. O. Collin is with Snecma Moteurs, RN7, BP 81, Evry 91003 Cedex, France. P. Aubry and T. Dubois are with the Cooperation Laser Franco-Allemande, 16 bis avenue Prieur de la Cote d'Or, Arcueil 94114, France. M. Hogstrom and P. Nylen are with the University of Trollhattan/Uddevalla, Gustavamelinsgata 6, 461 29 Trollhattan, Sweden. P. Jonsson is with the Volvo Aero Corporation, SE-461 81, Trollhattan, Sweden.

Received 20 July 2004; revised manuscript received 18 January 2005; accepted 11 February 2005.

0003-6935/05/193869-08$15.00/0

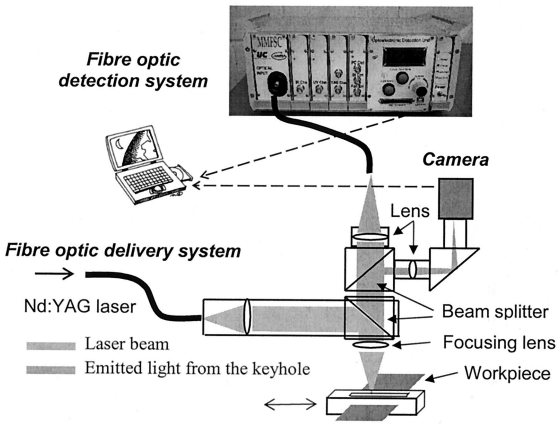


Fig. 1. Schematic of experimental arrangement.

ages to be observed at higher temporal resolution. However, it has been demonstrated that, similar to the single-point photodiode analysis,[8,9] the degree of partial penetration can be monitored by using the intensity of the keyhole emissions obtained from a coaxial observation.[10–12] Taking advantage of the spatial resolution capability of the camera sensor, full penetration can also be observed as the presence of an intensity minimum in the keyhole region.[11–14] It has also been demonstrated that it is possible to detect deviations from the desired path, seam width and weld spatters.[11–12]

In this paper we describe optical techniques based on the analysis of signals detected with both a camera and a single-point sensor, allowing real-time monitoring of full penetration. Statistical, spectral analyses and different image processing techniques are tested. We investigate their relative merits for preventing the formation of a hole while maintaining full penetration when welding variable thickness workpieces at high power.

## 2. Experimental Setup

The sensor arrangement is shown schematically in Fig. 1. The arrangement is based on coaxial detection of the light generated within the welding interaction zone, where the laser beam is focused onto the workpiece, creating the welding keyhole. The majority of the light produced by the welding process emerges from within this keyhole region. There is also a plume, that is visible above the keyhole, but this is much less bright. The keyhole light is detected by using both a large-core optical fiber plus photodiodes and a high-speed camera. The fiber optic detection system allows detection at a high temporal bandwidth, but averaged over the area of the keyhole entrance, whereas the camera is used to provide a high spatial resolution, but at a lower speed. Both systems are mounted directly at the welding head, and two identical beam splitters are used to collect the emitted light.

The fiber optic detection system consists of a standard fused silica large-core optical fiber with a core diameter of 600 μm. A lens is used to couple the light emitted by the welding process into the fiber. Its focal length and diameter (200 and 50 mm, respectively) are the same as that of the laser focusing lens, and so it images the workpiece with a ratio of 1:1. The light is delivered through the fiber to a detection box whose design was the subject of previous articles.[15,16] Inside the optical detection box the process radiation is split into three spectral ranges: 0.40–0.71 μm (UV/visible), 1.21–1.67 μm (IR), and 1.06 ± 0.01 μm (Nd:YAG). Each one is focused onto a different photodiode and then amplified by a separate amplifier module. A further module subtracts the UV/visible signal from the IR and thus provides a signal that is related to the deviation from the optimum focus position. This module allows the detection of a focal error in the range of few millimeters with an accuracy of ±0.3 mm.[16] It exploits the chromatic aberrations of the lenses that couple the two wavelengths of light into the fiber with different efficiencies. Following this focal error module, another module is able to provide a real-time control signal to drive the translation stage of the laser head focus with the correct amplitude swing. The optical detection unit incorporates user-friendly features. The included software provides an iterative algorithm, which takes only a few hundred milliseconds to complete, seeking the optimum amplifier gains for a specific welding condition or laser arrangement. This way, costly reference welds after the installation of the system or on new materials can be significantly reduced. It includes analog-to-digital converters for the signals of the three channels and the focal error output, with a bandwidth of 10 kHz. A universal serial bus connection to an external computer also makes it possible to record all data and enables further signal processing in real time.

The second sensor uses a camera to view the weld on axis. First, image recording was carried out at up to 2000 frames/s for a 256 × 256 pixel high-speed CMOS camera (Photron Ultima 1024). We subsequently recorded keyhole images from a CCD digital camera at 30 frames/s (Unibrain Fire i-400) permitting signal processing in real time.

A Nd:YAG laser system (either TRUMPF 4 kW or Rofin Sinar, 2.5 kW) was used to weld Inconel 718 and titanium (Ti-6A1-4V). All experiments have been realized at constant speed and are bead-on-plate welds. A critical aspect of welding titanium or nickel alloy is the gas protection against oxidation. Welding was therefore carried out with the workpiece inside an argon-filled closed box, ensuring good protection on both sides of the workpiece.

## 3. Offline Development of the Techniques

The ability to detect and use the optical emissions from the weld-pool area for penetration monitoring and control has been examined by many authors.[1–9] It has been shown that there exists a linear correlation between the penetration depth and the light emitted from the weld-pool area coaxially with the laser beam during partial penetration welding conditions. In our application, the welds are required to be

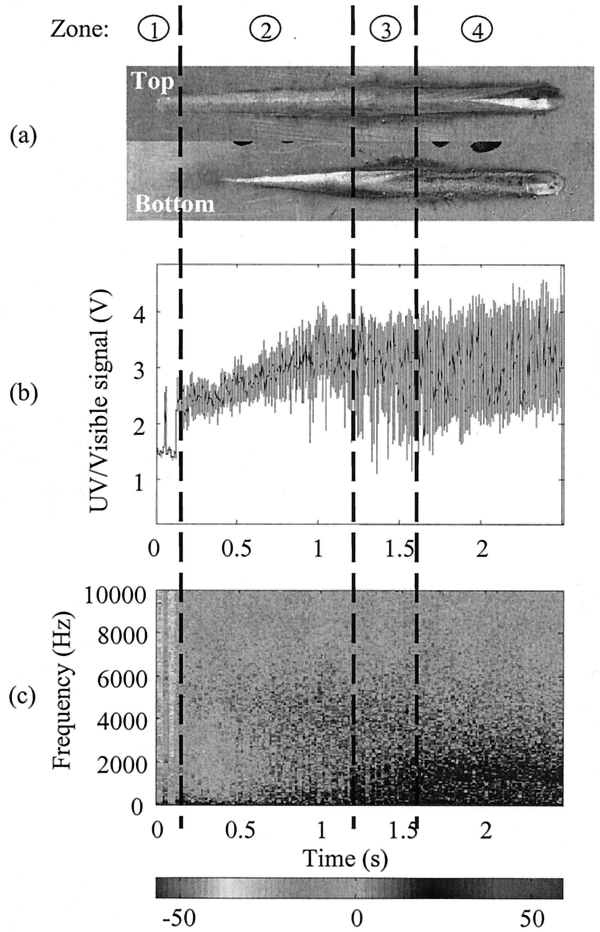


Fig. 2. (a) Photograph of top and bottom surface of weld produced in 2 mm thick Inconel at a speed of 1.2 m/min, (b) UV/visible signal detected by the detection box during welding. (c) Spectrogram calculated from the UV/visible signal.

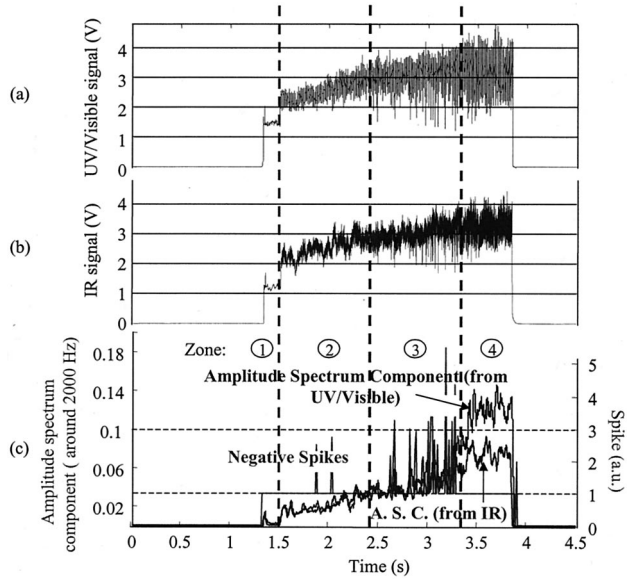


Fig. 3. (a) UV/visible and (b) IR signals detected by the detection box during welding for an increase of the laser power while the laser beam is moving at a speed of 1.2 m/min (2 mm thick Inconel). (c) Amplitude spectrum component and negative spike content calculated from the UV/visible and IR signals (threshold level $T = 1.8$).

fully penetrating (i.e., to extend completely through the thickness of the material). We are therefore concentrating on techniques to ensure full penetration.

### A. Single-Point Sensor

With a keyhole welding process, a weld will always be fully penetrated if the welding keyhole fully penetrates the material. In such a case, the keyhole naturally oscillates at a characteristic frequency of a few kilohertz, dependent on the thickness of the material.[5,6,17] The bandwidth of the optical detection unit was set to 10 kHz, allowing these frequencies to be recorded. Figure 2 shows the UV/visible signal and its Gabor spectrogram obtained by using a 512-point sliding Hanning window, in order to show the frequency content of the time series as a function of time. The weld was obtained by changing the laser power while moving the beam at a constant speed. When the weld starts, it is only partially penetrating with a slow increase in depth with power (zone 1).

This is a conduction-limited welding region, and a sharp increase in the UV/visible signal is detected (transition to zone 2) when a keyhole starts to form, and the coupling of the laser into the workpiece is hence significantly enhanced. In zone 2, penetration increases quickly with power until full penetration is achieved. The UV/visible signal increases with laser power throughout zone 2, until the keyhole starts to penetrate through the rear of the workpiece (zone 3). The presence of spatters at the rear of the workpiece in zone 4 confirms the presence of a stable fully penetrated keyhole. A broadband modulation spectrum when the rear of the keyhole opens (zone 3) changes to a distinct frequency peak around 2000 Hz in zone 4 for a fully penetrating keyhole Fig. 2(c).

This measurement does not suffer from the amplitude variations of the optical signals and can be obtained by performing a standard fast Fourier transform. The amplitude of the frequency content in a range between 1600 and 2400 Hz is shown in Fig. 3 for the UV/visible and IR signals. Analysis of the frequency spectrum of the two detected signals can be used to show the presence of an opened keyhole. As shown in Fig. 3, the UV/visible and IR signals are similar and their spectra exhibit a similar trend, i.e., a clear increase of content in the 1600–2400 Hz range in the presence of an opened keyhole. This increase is, however, lower in the case of the IR signal. This can be explained by the fact that the IR and UV/visible signals derive from different physical aspects of the welding process (visible and UV radiations arise from atomic transitions and Bremsstrahlung radiation within the plasma plume, while IR blackbody radiation is emitted from both the hot plasma plume and the molten material) but also in our case by the level of noise coming from the photodiodes used for the recording of each signal. The gain necessary to record the UV/visible signal was 30–50 times higher than

that used for recording the IR signal, resulting in increased noise. In addition, as confirmed by the clarity of the recorded keyhole image presented below, the plasma plume intensity was kept low (mainly because of the shielding gas).

However, this kind of weld requires a large amount of energy (to open the keyhole at the rear) and can become unstable, while a fully penetrated weld can be achieved without an opened keyhole, allowing an increase of the work speed or a decrease of the laser power. The signal also contains information on the imminent opening of the keyhole. As can be seen in Figs. 3(a) and 3(b), there exist some significant negative spikes in zone 3. These negative spikes correspond to a very fast decrease of the reflected light and occur when the keyhole momentarily penetrates through the workpiece. They tend to be less apparent in the case of a fully opened keyhole because of the higher frequencies generated by the keyhole oscillations, as shown in Figs. 2, 3, and 7. A parameter has been derived to detect this phenomenon by comparing the minimum with the maximum of a set of data (IR or UV/visible signal) relative to the mean of this set:

$$\text{Spike} = [(\langle y \rangle - \min(y)) - T(\max(y) - \langle y \rangle)], \quad (1)$$

where $\langle y \rangle$ is the arithmetic mean of the set of data $y$, $\min(y)$ is the minimum element of $y$, $\max(y)$ is its maximum element, and $T$ is the threshold level ($>1.5$).

This calculation normalizes the signal such that if there are no spikes present a value of 1 is generated during the weld. A negative spike on the IR (or UV/visible) signal is transformed into a positive deviation away from this nominal value of 1, with the height of this deviation proportional to depth of the negative spike. The signal is equal to 0 when there is no signal from the sensor (i.e., no welding is taking place). The region where the spikes are densest corresponds to the part of the weld where the keyhole is opening and closing at the rear; if fully closed (or fully opened), no spikes are observed. The same number of spikes are observed, whichever signal is analyzed (UV/visible or IR not plotted). Meanwhile, spectral analysis shows that more than 10% of the UV/visible light recorded oscillates around 2000 Hz when welding is fully performed in a fully opening keyhole regime. Combining both analysis techniques provides a more robust measurement; if the number of spikes is reduced and the spectrum signal increases, then the laser power should be decreased (or speed increased). However, if the number of spikes decreases and the spectral component does not increase, then the laser power should be increased (or speed decreased).

### B. Camera

The signals recorded by photodiodes offer very good temporal resolution but poor spatial resolution. Good spatial resolution can be achieved by imaging the keyhole onto a camera sensor chip. Cameras with

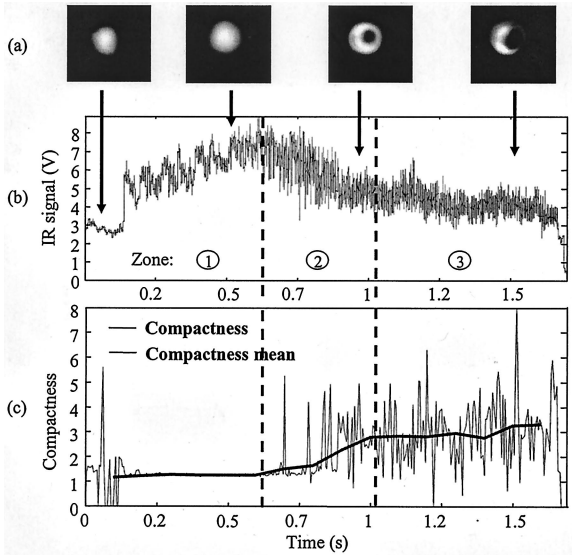


Fig. 4. (a) Keyhole images recorded when 2-mm-thick bead-on-plate titanium was welded at a speed of 1.8 m/min. (b) IR signal detected by the detection box. (c) Compactness coefficient calculated from the keyhole images. The bold curve is a running average of the compactness coefficient. The zero value corresponds to an entire black image. The weld has been produced by increasing the laser power with a constant speed.

frame rates of up to 4000 frames/s have been available for few years. However, although high for a camera system, such a frame rate is still less than that required for detection of the keyhole oscillation frequencies referred to above and such a large amount of data is difficult to process in real time. Alternative image analysis techniques are hence required. We used a CMOS camera at 2000 frames/s for the prototyping step of the image processing.

The light emitted from the keyhole during a partial or a weakly fully penetrated weld has an almost circular shape, as can be seen on the two images plotted in zone 1 in Fig. 4(a). When a fully penetrated keyhole occurs, the bright light emitted from the welding keyhole has a dark region in the center [Fig. 4(a), zone 2 and 3]. The donut shape, which appears when only a small amount of light penetrates the workpiece, becomes a crescent shape as the laser power increases. The compactness coefficient is one way of differentiating between these shapes. We defined this coefficient as

$$\text{Compactness} = \frac{(\text{Perimeter})^2}{\text{Area} \times 4\pi}. \quad (2)$$

Compactness = 1 for an exact circular shape and is significantly larger than 1 in the case of a crescent shape. This compactness coefficient is plotted in Fig. 4(c) for the weld produced with increasing laser power at constant speed. In zone 1, where the weld is either partially penetrating or just starting to fully penetrate, the compactness has a rough constant value of approximately 1.3. Its average value (at 20 Hz) increases as the keyhole starts to open at the

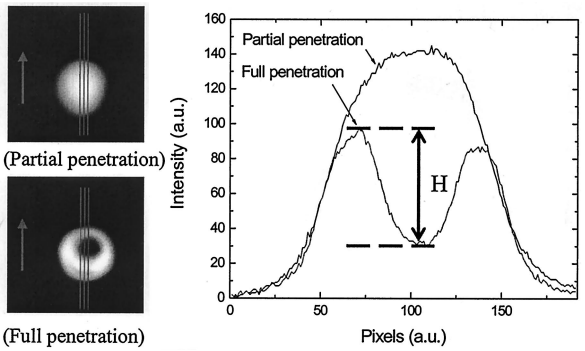


Fig. 5. Images of the keyhole and their corresponding intensity profile. The intensity profile represents the average profile along the three lines.

rear (zone 2) to reach almost 3 (zone 3) when the keyhole is fully opened. It is clear, however, that averaging is essential if this coefficient is to be used as the basis of a process monitor at this frame rate.

Based on the calculation of compactness, we have developed an image processing algorithm that allows detection of the welding regime:

Zone 1. No hole inside an almost circular keyhole (Compactness coefficient around 1.3),

Zone 2. Presence of a significant hole inside an almost circular keyhole (Compactness coefficient less than 3).

Zone 3. No significant hole inside a "crescent" keyhole (Compactness coefficient around 3).

However, this method requires the binarization of the keyhole image. We observed that it is sensitive to the quality of the images (coming from plume interference, oxidation, material) and the choice of the threshold value is not easy. An alternative technique based on the calculation of the intensity profile of the keyhole has therefore been investigated.

Figure 5 shows an example of a keyhole image when welding is performed in both partially and fully penetrated regimes. When the keyhole is fully penetrated, the camera image shows a circular shaped intensity minimum roughly in the center of the keyhole. It is possible to follow the degree of the full penetration by focusing on the depth of the intensity minimum. We therefore defined the normalized depth coefficient $H$ as follows:

$$H = 100(I_{\max} - I_{\min})/(I_{\max}), \tag{3}$$

where $I_{\max}$ and $I_{\min}$ are the maximum and the minimum of the intensity, respectively. The normalization avoids sensitivity to intensity changes coming from a new material or change in the quality of the images (including plume vapor interference, blooming effect, oxidation or change on another laser head).

Figure 6 shows the normalized coefficient $H$ obtained for the weld presented in Fig. 4. In a partially penetrating regime (zone 1), $H$ is null. As the weld becomes rapidly overpenetrated, $H$ reaches 80%–100%

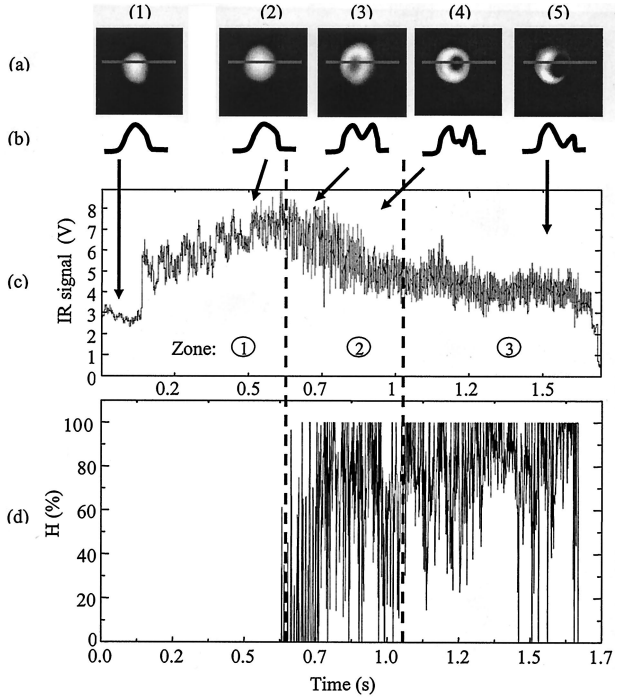


Fig. 6. (a) Keyhole images recorded when 2-mm-thick bead-on-plate titanium was welded at a speed of 1.8 m/min. (b) Sketches of their intensity profiles. (c) IR signal detected by the detection box. (d) Depth coefficient $H$ calculated from the keyhole image intensity profile. The weld has been produced by increasing the laser power with a constant speed (same weld as presented in Fig. 4).

in zone 2 and 3. The optimum penetration is obtained at the beginning of zone 2, when $H$ is around 30.

## 4. On-Line Results and Discussion

Techniques developed off-line have been transferred on-line by using National Instruments LabVIEW software. A data acquisition card (including 12 bits input with a sampling rate up to 500 ksamples/s) was used on a 2 GHz CPU laptop under Windows XP. However, the USB connection of the optical detection unit is able to provide data fast enough to avoid the use of such a data acquisition card. Images have been grabbed from a standard FireWire port.

Figure 7 presents the real-time sensor results of a weld obtained by increasing the laser power from 1.4 to 1.9 and 2.4 kW in steps at constant speed.

The program developed is able to display in real time the IR and UV/visible signals measured by the detection unit. It calculates the spike content of both signals (Only the IR spike content is shown in Fig. 7(c), since UV/visible spike content is similar) and the amplitude spectrum weight in the frequency range between 1600 and 2400 Hz [Fig. 7(d)]. The data are acquired into a circular buffer at 14,000 samples/s. They are retrieved at the same time in sets of 2048 samples for data processing. The processing time is fast enough to provide a real-time response. The photograph of the rear of the workpiece shows that for a laser power of 1.4 kW the penetration is partial with no weld ob-

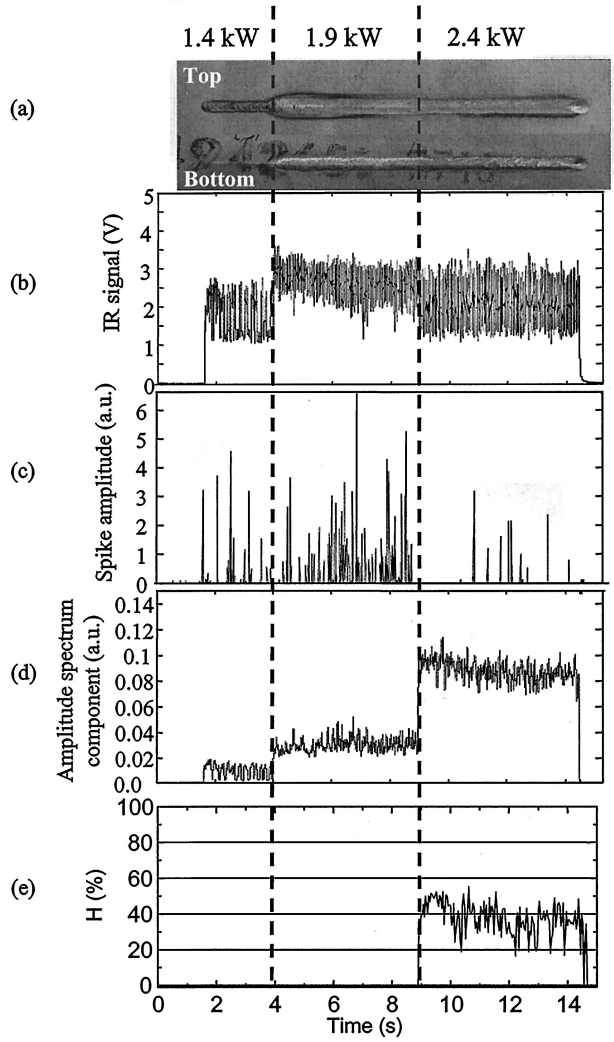


Fig. 7. (a) Photographs of top and bottom surface when 1.6-mm-thick bead-on-plate Inconel was welding for three laser powers (1.4, 1.9, and 2.4 kW) at a speed of 0.6 m/min. (b) IR signal recorded by the detection box. (c) Amplitude of the spikes calculated in real time from the IR signal. (d) Amplitude of the spectrum component in the frequency range between 1600 and 2400 Hz calculated in real time from the IR signal. (e) Keyhole opening depth coefficient calculated in real time from the images.

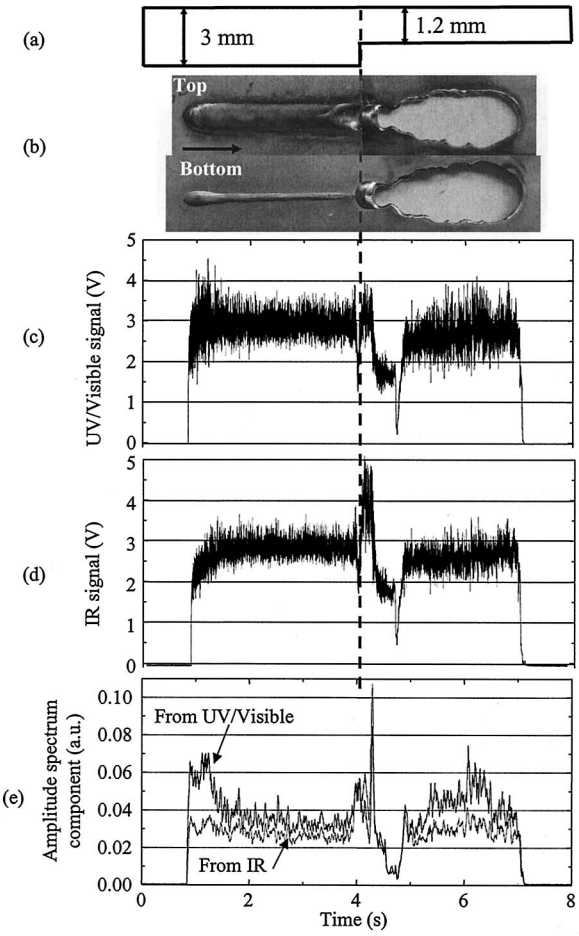


Fig. 8. (a) Longitudinal cross section of the Inconel stepped workpiece; (b) Photographs of top and bottom surface when bead-on-plate Inconel was welded at constant laser power and at a speed of 0.6 m/min; (c) UV/visible and (d) IR signals recorded by the detection box; (e) Amplitude of the spectral component in the frequency range between 1600 and 2400 Hz calculated in real time from the UV/visible and IR signals.

servable. Fully penetrated welding is achieved for a laser power >1.9 kW, while a fully penetrated keyhole does not occur until the laser power reaches 2.4 kW, confirmed by the presence of spatters on the rear surface of the workpiece.

The analysis of the presence of spike is a less clear indication of the imminent opening of a keyhole compared with our previous off-line data. Some negative spikes are detected at all power levels. However, they are clearly predominant in the region corresponding to a fully penetrated weld without a fully opened keyhole. The amplitude spectrum coefficient in the frequency range between 1600 and 2400 Hz reaches 10% for the maximum power. It clearly detects the natural modes of oscillations of a fully opened keyhole.

Keyhole images of the same weld have been recorded and processed at 30 Hz in parallel. The keyhole opening depth coefficient $H$ is 40% for a 2.4 kW laser power confirming a keyhole opening [Fig. 7(e)]. The compactness coefficient was also computed for each image (not plotted). It is very unstable during both partial penetration and fully opening regime, since the size and the shape of the keyhole images fluctuates considerably. No crescent shape has been observed. To conclude, the behavior of this parameter is unsuitable for following the degree of penetration, mainly due to the image quality, which can not be readily enhanced.

The analysis techniques were also tested by introducing an alternative perturbation: changes of the workpiece thickness. Figure 8 shows UV/visible, IR and their respective amplitude spectrum signals when an overpenetration leading to the formation of a hole occurs, because of the excess laser power (and a too low-welding speed). When the laser is welding the 3-mm-thick part, the keyhole is not

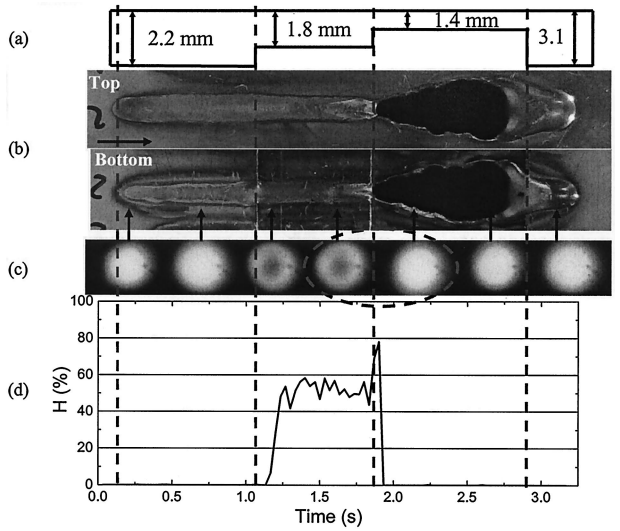


Fig. 9. (a) Longitudinal cross section of the Inconel stepped workpiece. (b) Photographs of top and bottom surface when welding bead-on-plate Inconel at constant laser power and at a speed of 0.9 m/min. (c) Keyhole images recorded at 30 Hz. (d) Keyhole opening depth coefficient $H$. The region around the highlighted images is shown in more details in Fig. 10.

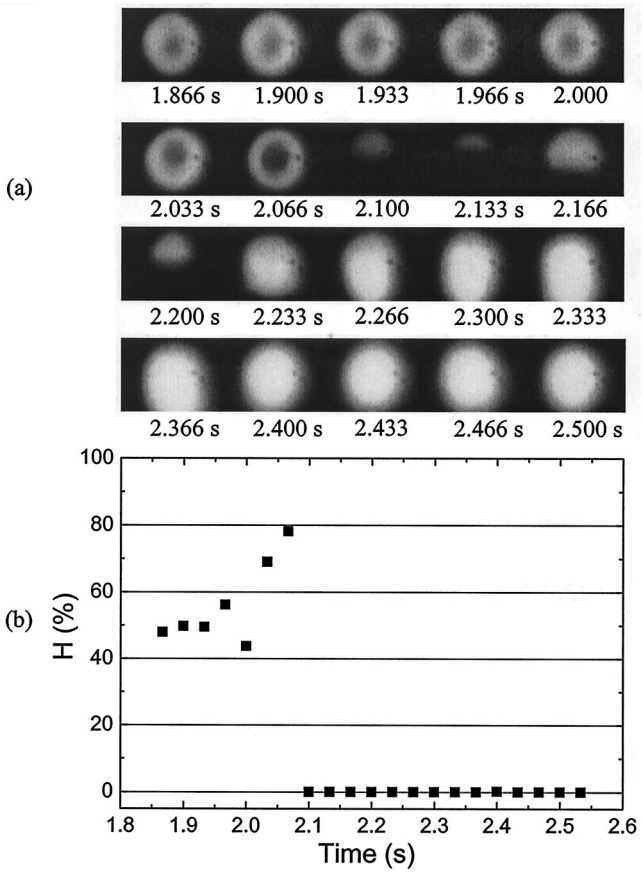


Fig. 10. (a) Sequence of keyhole images at the 1.8–1.4-mm-thick interface. (b) Keyhole opening depth coefficient $H$ calculated in real time for each frame (30 Hz).

fully opened. However, when the laser beam reaches the 1.2-mm-thick part, the amplitude of the 1600–2400 Hz spectral component increases as expected in each case to 10%, which corresponds to a fully opened regime. These components both fall quickly to 1% when the hole is formed but then recover to a level similar to that obtained for a partial penetration. As shown in Fig. 8(b), however, a large hole is obtained along the entire second part of the weld. An increase of the IR emission is observed during welding at the interface between the two thicknesses, but this was not be observed for all our trials on similar workpieces. Only the general decrease of the average UV/visible and IR signals gives evidence of the burnthrough. Observation of the amplitude spectrum is hence clearly unable either to see a hole or to prevent its formation, since no strong overpenetration can be interpreted from the signal. Instead the signal may be misinterpreted as a partial penetration, clearly a problem for any control system. The amplitudes of the UV/visible and IR signals recorded when the hole is forming suggests that the plasma plume and the molten pool emission intensity stay relatively constant despite the total collapse of the keyhole.

Keyhole images present a similar behavior, as shown in Fig. 9, when a 2.1-1.8-1.4 mm stepped Inconel workpiece is welded. A fully opened keyhole is reached in the 1.8-mm-thick part (with $H$ around 50). When the laser beam launches the 1.4-mm-thick part, a hole is formed. The keyhole images show, first, a keyhole opening becoming very great, reaching 80%. A few milliseconds later, since the laser power and speed are kept constant, the keyhole images change aspect and become similar to what is obtained in a partial penetration regime, i.e., a single-peak intensity profile (with $H = 0$). However, a large hole is formed along the entire weld on this thickness. Figure 10 shows the detail of keyhole images and the corresponding depth coefficient $H$ at the interface 1.8–1.4 mm. Two images show $H > 70\%$ (at 2.033 and 2.066 s). Then a large amount of light penetrates through the plate, corresponding to four almost completely black images. However, they are interpreted as a partial penetration regime. The system is able to see the formation of a hole on only two frames at 30 Hz. Trials with a 100 Hz frame rate camera have hence been carried out. They show that six frames present an $H$ coefficient $> 60\%$. Provided that the control system reduces the laser power sufficiently quickly, a hole can thus be avoided. Unfortunately, the system is unable to follow the hole presence once it is formed. Surprisingly, both sensor results show a level of light emitted (UV/visible and IR) and a keyhole geometry similar for both a burnthrough and a partial penetration. We found no clear explanation for this phenomenon; further investigation (possibly by viewing the keyhole and melt pool from different angles) could perhaps improve our understanding of this process.

This technique has been successfully used to maintain a full penetration (i.e., without overpenetration or lack of penetration) by controlling the laser power in the presence of linear and step changes of workpiece thickness.[18] The system developed reacts quickly

enough to avoid the formation of a hole by decreasing the laser power proportionally to the degree of keyhole opening. This technique is sufficiently robust to work even if the images are foggy and computational time is short (<10 ms). However, a limitation of this technique is that it is unable to distinguish between a fully penetrated weld obtained without an opened keyhole and a partially penetrated weld, restricting its range of operation. However, this is not such a problem, as a fully opened keyhole is generally preferred, as it leads to welds with reduced porosity. In parallel, a focus feedback control based on a previously developed technique[15] has been successfully tested from the optical detection unit signals.[16,18]

## 5. Conclusion

Optical techniques which allow real-time monitoring of the weld penetration in Inconel and titanium have been presented. They are based on two optical sensors: a camera and a single-point sensor, both viewing the welding keyhole coaxially. Experimental tests have shown that the frequency content of the signal from the single-point sensor clearly indicates the presence of a fully opened keyhole, thus ensuring a fully penetrated weld. The presence of negative spikes shows a more limited correspondence with the imminent opening of the keyhole. Techniques based on the image processing of the camera images have demonstrated the ability to follow the degree of full penetration by analysis of the intensity profile. An alternative image processing technique based on keyhole shape recognition has been developed, but it is unreliable if the image has poor contrast, which can arise because of the welding plume.

An interesting phenomenon has been observed during the formation of a hole, occurring when welding with a high laser power on a thin workpiece. Both the single-point and camera signals indicate partial penetration welding after a very brief transition phase. However, the $H$ parameter is robust enough to properly interpret the transition phase signal as a hole in formation, which was not possible with the single-point sensor techniques.

The software developed is easy to use, and the key internal parameters can be readily modified in order to ensure successful operation as welding parameters are changed. It can hence provide the feedback control of the laser power in order to maintain a full penetration and to avoid overpenetration.

The authors acknowledge the support of the European Commission, which has provided enabling funds through the project MMFSC (Manufacturing and Modeling of Fabricated Structural Components). We are also grateful to A. Campo and J. L. Rodríguez for their technical input and Manuel Trucco for fruitful discussions.

## References

1. J. Beersiek, "New aspects of monitoring with a CMOS camera for laser materials processing," in *Proceedings of the International Congress on Applications of Lasers and Electro-Optics* (Laser Institute of America, 2002).
2. R. Guttler, "Sensor detects faults in keyhole," Opt. & Laser Europe **10,** 13–15 (1998).
3. C. Bagger and F. O. Olsen, "Laser welding closed-loop power control," J. Laser Appl. **15,** 19–24 (2003).
4. J. Ortmann, E. W. Kreutz, C. Maier, T. Wehner, M. Kogel-Hollacher, S. Kaierle, and R. Poprawe, "Online detection of defect classes for laser beam welding," in *Proceedings of the International Congress of Applications of Lasers and Electro-Optics* (Laser Institute of America, 2003).
5. F. M. Haran, D. P. Hand, S. M. Ebrahim, C. Peters, and J. D. C. Jones, "Optical signal oscillations in laser keyhole welding and potential application to lap welding," Meas. Sci. Technol. **8,** 627–633 (1997).
6. H. Gu and W. W. Duley, "Discrete signal components in optical emission during keyhole welding," in *Proceedings of the International Congress of Applications of Lasers and Electro-Optics* (Laser Institute of America, 1997), **83,** Part 1, Sect. C, pp. 40–46.
7. A. Sun, E. Jr. Kannatey-Asibu, and M. Gartner, "Monitoring of laser weld penetration using sensor fusion," J. Laser Appl. **14,** 114–121 (2002).
8. P. Sanders, K. Leong, J. Keske, and G. Kornecki, "Real-time monitoring of laser beam welding using infrared weld emission," J. Laser Appl. **10,** 205–211 (1998).
9. S. Postma, R. G. K. M. Aarts, and A. J. F. M. Hesemans, "Penetration feedback control in overlap laser welding of sheet metal," in *Proceedings of WESIC* (University of Twente, 2001), pp. 495–503.
10. J. Beersiek, R. Poprawe, W. Schulz, H. Gu, R. E. Mueller, and W. W. Duley, "On-line monitoring of penetration depth in laser beam welding," in *Proceedings of the International Congress of Applications of Lasers and Electro-Optics* (Laser Institute of America, 1997), Vol. **83,** Part 1, Sect. C, pp. 30–39.
11. S. Kaierle, P. Abels, G. Kapper, C. Kratzsch, J. Michel, W. Schulz, and R. Poprawe, "State of the art and new advances in process control for laser materials processing," in *Proceedings of the International Congress of Applications of Lasers and Electro-Optics* (Laser Institute of America, 2001).
12. C. Kratzsch, P. Abels, S. Kaierle, R. Poprawe, and W. Schulz, "Coaxial process control during laser beam welding of tailored blanks," in *Proceedings AHPLA99, High-Power Lasers in Manufacturing*, X. Chen, T. Fujioka, and A. Matsunawa, eds., Proc. SPIE **3888,** 472–482 (2000).
13. J. Beersiek, "A CMOS camera as a tool for process analysis not only for laser beam welding," in *Proceedings of the International Congress of Applications of Lasers and Electro-Optics* (Laser Institute of America, 2001).
14. J. Petereit, P. Abels, S. Kaierle, C. Kratzsch, and E. W. Kreutz, "Failure recognition and online process control in laser beam welding," in *Proceedings of the International Congress of Applications of Lasers and Electro-Optics* (Laser Institute of America, 2002).
15. F. M. Haran, D. P. Hand, C. Peters, and J. D. C. Jones, "Focus control system for laser welding," Appl. Opt. **36,** 5246–5251 (1997).
16. A. Cobo, F. Bardin, P. Aubry, W. Knapp, O. Collin, J. D. C. Jones, D. P. Hand, and J. M. López-Higuera, "Optical fibre-based focus control system for laser welding incorporating automatic setup," in *Proceedings of 16th International Conference on Optical Fiber Sensors*, K. Hotate and H. Nagai, eds. (Institute of Electronics, Information and Communication Engineers, 2003), pp. 412–415.
17. T. Klein, M. Vicanek, J. Kroos, I. Decker, and G. Simon, "Oscillations of the keyhole in penetration laser beam welding," J. Phys. D **27,** 2023–2030 (1994).
18. F. Bardin, A. Cobo, J. M. Lopez-Higuera, O. Collin, P. Aubry, T. Dubois, M. Högström, P. Nylen, P. Jonsson, J. D. C. Jones, and D. P. Hand, "Closed-loop power and focus control of laser welding for full penetration monitoring," Appl. Opt. **44,** 13–21 (2005).